THE ASTROPHYSICAL JOURNAL, 558:185–193, 2001 September 1

SOLID CARBON DIOXIDE IN REGIONS OF LOW-MASS STAR FORMATION

A. NUMMELIN,[1] D. C. B. WHITTET, AND E. L. GIBB
Department of Physics, Applied Physics, and Astronomy, and New York Center for Studies on the Origins of Life, Rensselaer Polytechnic Institute, Troy, NY 12180
P. A. GERAKINES
Department of Physics, University of Alabama at Birmingham, 1300 University Boulevard, Room 310, Birmingham, AL 35294
AND
J. E. CHIAR[2]
NASA Ames Research Center, Mail Stop 245-3, Moffett Field, CA 94035
Received 2000 December 27; accepted 2001 May 8

ABSTRACT

We present high-resolution ($R \sim 1500$–2000) spectra of the 4.27 μm asymmetric stretching feature of solid CO_2 in eight lines of sight observed with the Short Wavelength Spectrometer of the *Infrared Space Observatory*. Two of the sources are field stars located behind the Taurus molecular cloud; the others are young stellar objects (YSOs) of predominantly low-to-intermediate mass. We find a significant source-to-source variation in the solid CO_2/H_2O abundance ratio in our sample: two lines of sight, Elias 18 and RAFGL 989, have CO_2 abundances of $\sim 34\%$–37%, considerably higher than in other lines of sight studied to date. In agreement with a previous study of Elias 16, we confirm a substantial ($\sim 20\%$) abundance of solid CO_2 relative to H_2O in the quiescent intracloud medium. We compare the CO_2 profiles with laboratory spectra of interstellar ice analogs from the Leiden Observatory Laboratory database. Results show that the 4.27 μm profiles toward field stars and embedded low-mass objects are remarkably similar to each other and seem to originate mostly in cold H_2O-rich ice. In two higher mass YSOs (RAFGL 989 and S255 IRS1), the profiles are clearly different, and at least the latter source shows signs of thermal processing.

Subject headings: dust, extinction — infrared: ISM — ISM: abundances — ISM: lines and bands — ISM: molecules

1. INTRODUCTION

1.1. *General*

Observations with the *Infrared Space Observatory* (*ISO*) have shown carbon dioxide (CO_2) to be one of the major constituents of the ice mantles that coat dust grains in lines of sight toward virtually all embedded young stellar objects (YSOs) observed to date (de Graauw et al. 1996a; Gürtler et al. 1996; Gerakines et al. 1999). CO_2 is much less volatile than, for example, CO and may exist in solid form up to ~ 100 K before sublimation. It can therefore be used to probe interstellar ice under a wider range of physical conditions. Abundant solid CO_2 has also been detected in the line of sight of the star Elias 16 (Whittet et al. 1998), located behind the Taurus molecular cloud (TMC), a result that challenges theories proposing CO_2 formation by energetic processes (see § 1.2). Gas-phase CO_2 has also been found but so far only at low abundance in most lines of sight (Boonman et al. 2000; van Dishoeck et al. 1996). An exception is the Herbig Ae/Be system LkHα 225, toward which most or all of the CO_2 appears to be in the gas phase (van den Ancker et al. 2000).

CO_2 has no permanent dipole moment and, consequently, lacks rotational electric dipole transitions. There are two active fundamental vibrational modes of solid CO_2 in the mid-infrared: the asymmetric stretching mode (denoted ν_3) at 4.27 μm (2340 cm^{-1}) and the doubly degenerate bending mode (denoted ν_2) at 15.2 μm (660 cm^{-1}). The intrinsic strength of the stretching mode exceeds that of the bending mode by a factor of 7. Carbon dioxide in the Earth's atmosphere prevents ground-based observations of both of these bands. In addition to features arising in the common isotopic form, $^{13}CO_2$ has an observable ν_3 stretch mode at 4.38 μm (2283 cm^{-1}).

Because of the degenerate nature of the ν_2 bending mode, it is more sensitive than the ν_3 stretch to the molecular environment and is thus potentially more useful for constraining the properties of the ice mantles (Ehrenfreund et al. 1996). However, considering (1) the 7 times lower intrinsic band strength of the bending mode relative to the stretch mode; (2) the lower sensitivity of the *ISO*-SWS (Short Wavelength Spectrometer) system at 15 μm, in conjunction with the residual periodic instrumental modulation (fringing) often present in 15 μm standard processed SWS data; and (3) the relatively low mid-infrared flux levels toward low-mass YSOs and field stars, there are cases where reliable data on CO_2 can be obtained in the 4.27 μm band only. We focus on such cases in this paper. Our sample of objects lacking 15 μm data naturally contains lower luminosity sources than those typically studied to date: our source list includes two field stars, five embedded low- and intermediate-mass YSOs, and one more massive YSO. It is important to study what constraints can be put on ice properties and to evaluate CO_2 abundances in such objects, notwithstanding the lack of mid-infrared data. This is the goal of the present paper.

1.2. *Chemistry of* CO_2

Interstellar CO_2 is formed by oxidation of CO. This could potentially occur in the gas phase or on the surface of

[1] Present address: Department of Electrical and Computer Engineering, Chalmers Lindholmen University College, P.O. Box 8873, SE-40272 Gothenburg, Sweden.
[2] Also at SETI Institute, Mountain View, CA 94043.

icy dust grains, with or without the influence of ultraviolet radiation or high-energy ion bombardment. Under simulated interstellar conditions in the laboratory, CO_2 is easily formed through UV photolysis of ices containing H_2O and CO (d'Hendecourt et al. 1986; Sandford et al. 1988):

$$H_2O + h\nu \rightarrow H_2O^* \rightarrow OH^* + H\ , \quad (1)$$

$$OH^* + CO \rightarrow H + CO_2\ . \quad (2)$$

Some recent computational models of interstellar chemistry, however, have difficulties producing CO_2 this way (Ruffle & Herbst 2001, and references therein). Laboratory studies of photolyzed ices have also shown that CO_2 can be produced through diffusive grain surface reactions, such as

$$CO + O \rightarrow CO_2\ , \quad (3)$$

$$O + HCO \rightarrow CO_2 + H\ , \quad (4)$$

$$CO + OH \rightarrow CO_2 + H\ . \quad (5)$$

Experiments indicate that reaction (3) may possess a significant activation energy barrier (Grim & d'Hendecourt 1986), although this is in contrast to earlier results by Fournier et al. (1979). If there is indeed a significant activation barrier, quantum mechanical tunneling could still make this reaction proceed at the low temperatures of interstellar ice mantles, but the reaction probability will depend on the magnitude of the barrier. It is also possible that UV dissociation of H_2O could produce oxygen atoms with excess energy that could help overcome any activation barrier and thus drive the reaction forward (d'Hendecourt et al. 1986; Grim & d'Hendecourt 1986), although dissociation of H_2O primarily leads to OH which can react with CO directly through reaction (5). The latter reaction has been studied under laboratory conditions (Frost, Sharkey, & Smith 1991) and could also be of some importance in the gas phase (Charnley & Kaufman 2000), although CO_2 is not predicted to be formed in any sizeable abundance in interstellar gas (e.g., Herbst & Leung 1986).

1.3. *Description of the Sources*

The objects providing the infrared continuum against which CO_2 absorption is observed in this study (Table 1) fall into two major categories. The first category of objects comprises field stars located behind the dark cloud medium. This group includes the *K*-type giants Elias 13 and Elias 16; the CO_2 absorption features detected along their lines of sight represent intervening interstellar icy dust grains in the TMC. Because of the nature of the TMC dark cloud, this ice is cold and little processed by radiation, stellar winds, and outflows, and has no significant interaction with the background star. These lines of sight are therefore rich in volatiles such as solid CO. The Taurus cloud is a particularly interesting low-mass star-forming region to study since it is nearby (140 pc) and free from shocks and internal luminous sources of ultraviolet radiation. The CO_2 absorption toward Elias 16 has previously been studied by Whittet et al. (1998) and Gerakines et al. (1999), but in order to make a fair comparison of this object with others in our sample, we have reanalyzed the data using the latest revision of the data processing pipeline (see § 2). This is particularly important since Elias 16 has low flux at 4.27 μm and therefore is sensitive to the adopted dark current (Whittet et al. 1998). The second category of objects—all other sources—consists of YSOs and pre–main-sequence stars that are more or less embedded. These objects are in evolutionary stages where most of their luminosity comes from nucleosynthesis rather than thermal collapse, but where stellar winds and outflows have not yet dispersed their natal molecular cloud, and they are therefore subject to high visual extinction. Absorption features observed toward these stars are assumed to be of partly or mainly circumstellar origin, rather than interstellar.

Elias 18, also in the TMC, is the illuminating star in the IC 2087 reflection nebula. The object is a highly obscured ($A_V \sim 15$–19) star faintly visible on the red Palomar plates; assuming it to be on the zero-age main sequence, the spectral type is ~B5 (Elias 1978). Tegler et al. (1995) suggest Elias 18 to be in transition between an embedded object and an exposed pre–main-sequence star. The large extinction in conjunction with observed CO bandhead emission indicates the presence of a circumstellar disk oriented close to edge-on (Shuping et al. 2001).

The Herbig-Haro object HH 100 in the nearby (~150 pc) R Coronae Australis molecular cloud is excited by a strong outflowing wind from an optically obscured ($A_V \sim 25$), variable infrared source denoted HH 100 IR, also known as R CrA IRS1 (Axon et al. 1982), which is located about 25″ northeast of the optical nebula. HH 100 IR is part of a cluster of newly formed stars in the R CrA cloud and is probably a pre–main-sequence star with a circumstellar

TABLE 1

Observed Lines of Sight and Observing Parameters

Object	Coordinates (J2000) R.A.	Coordinates (J2000) Decl.	Date	Revolution	λ Range (μm)	Type
Elias 13	04 33 25.9	26 15 33.9	1997 Sep 30	684	4.20–4.34	K2 III (field star)
Elias 16	04 39 38.9	26 11 26.8	1997 Oct 1	686	4.08–4.50	K1 III (field star)
Elias 18	04 39 55.7	25 45 02.4	1997 Oct 1	685	4.08–4.51	B5 ZAMS
S255 IRS1	06 12 53.8	17 59 21.9	1998 Mar 18	854	4.08–4.56	High-mass YSO system
RAFGL 989.....	06 41 10.1	09 29 35.8	1997 Nov 1	716	4.08–5.30	B2 ZAMS
HH 57 IRS.....	16 32 32.1	−44 55 28.6	1998 Mar 6	842	4.19–4.33	FU Ori
HH 100 IR	19 01 50.6	−36 58 08.9	1997 Oct 19	704	4.14–4.46	Class II YSO
R CrA	19 01 53.9	−36 57 09.7	1997 Oct 31	715	4.10–4.56	A5 IIe var (Herbig Ae)

Note.—Units of right ascension are hours, minutes, and seconds, and units of declination are degrees, arcminutes, and arcseconds.

disk (Bastien & Ménard 1990). R CrA itself is a Herbig Ae star, i.e., a pre–main-sequence star of intermediate mass (more massive than T Tauri objects) associated with circumstellar matter, molecular emission, and Balmer emission lines (e.g., Hillenbrand et al. 1992). It lies at the apex of the cometary reflection nebula NGC 6729.

HH 57 is located at a distance of about 700 pc in the Sa 187 dark cloud in Norma. It is excited by a strong infrared source, HH 57 IRS (Elias 1980; Reipurth & Wamsteker 1983), with a faint ($V \sim 17$) optical counterpart. Observations have shown this object to be a young, pre–main-sequence star of the rare FU Orionis type (Graham & Frogel 1985; Reipurth 1985) surrounded by large amounts of cool dust (Weintraub, Sandell, & Duncan 1991; Reipurth et al. 1993).

RAFGL 989 is a YSO located near the apex of the Cone Nebula in the NGC 2264 molecular cloud (Wynn-Williams 1982). Also known as NGC 2264 IRS1 and Allen's source, it lies within the positional error bars of the IRAS point source 06384+0932. The luminosity of this object is consistent with a 9.5 $M_\odot$ B2 zero-age main-sequence star (Allen 1972) with $A_V \sim 20$–30 (Thompson et al. 1998), which places it between high-mass YSOs such as Orion IRc2 and the lower mass objects in TMC. The star is presumably oriented pole-on (Schreyer et al. 1997).

One embedded object of higher mass, S255 IRS1, was included in the source sample as a control star. This YSO is located in a region with H II regions, fast outflows, OH and H_2O maser activity, and several sources of infrared and radio continuum, all of which indicate recent or progressing massive star formation. The YSO IRS1 is the most prominent of the infrared sources in the core of the S255 molecular cloud, and its emission measure indicates the presence of a compact or ultracompact H II region. High angular resolution observations (unresolved by *ISO*-SWS) reveal IRS1 to contain at least two pointlike IR sources 2.″6 apart, each probably located behind a dust disk or torus (Howard, Pipher, & Forrest 1997). In the context of this paper, the property that most significantly distinguishes high-mass from low-mass YSOs is the large amount of Lyman continuum in the former. Although S255 IRS1 was actually observed at 15 μm by the *ISO*-SWS, the poor signal-to-noise ratio (S/N) in this band precludes analysis of the CO_2 bending mode.

2. OBSERVATIONS AND DATA REDUCTION

The observations were made using the *ISO*-SWS as detailed in Table 1. Data were acquired for most sources using the astronomical observation template (AOT) SWS06, in which the grating is scanned at full spectral resolution with a resulting resolving power $R = \lambda/\Delta\lambda \sim 1500$–2000. The exception is RAFGL 989, for which AOT SWS01 (speed 3) was used at resolving power $\sim R/4$.

Data reduction was carried out in 2000 March at the Dutch *ISO* Data Analysis Centre, hosted by the Space Research Organization of the Netherlands in Groningen, using the Interactive Analysis software under IDL 5.3 on a Sparc/Sun workstation. All of the sources were reduced in a uniform way: we started at the edited raw data level and produced standard processed data (SPD) files using version 9.0 of the standard offline pipeline (see de Graauw et al. 1996b). The pipeline processing applied included a refined dark current subtraction for AOT Band 2A ($\lambda = 4.08$–5.30 μm, the only band considered in this paper) using the newly developed *Dynadark* module. No interactive adjustment of the dark current levels were therefore necessary in any of the sources. Corrections for pulse shape were also included in this version of the pipeline, improving the S/N and the removal of glitches (e.g., cosmic ray hits) from the data. The SPD thus produced were subsequently flat-fielded (zero-order), clipped at 3 σ from the median flux, and, finally, averaged and rebinned keeping an oversampling factor of 2. Remaining artifacts in the data, such as deviating fluxes and jumps, were identified by visual inspection and removed where necessary. No interactive processing was done. Up- and down-scans were treated separately throughout the data reduction. However, in all cases, the difference between the scan directions were found to be small, and we therefore used their combined average in the analysis.

The spectra were converted from flux to units of optical depth by ratioing each to its continuum. Data points with a flux S/N less than 3 σ were discarded from all data sets prior to this step. The spectral continua were determined by fitting local first-order polynomials to the data adjacent to the 4.27 μm feature (approximately 4.15–4.21 and 4.31–4.37 μm). The resulting spectra are shown in Figure 1. Toward two of the sources, Elias 16 and R CrA, the continuum is somewhat nonlinear, resulting in an apparent broad, shallow "emission bump" between 4.18 and 4.23 μm in Elias 16 and a somewhat oversubtracted continuum between 4.30 and 4.36 μm in R CrA. However, these effects are relatively small, and the polynomials fit the spectra well overall. In Elias 13 and HH 57 IRS, both of which have narrow wavelength coverage (4.19–4.34 μm), there are some uncertainties in the continuum level near the edges of the spectrum, and in both cases we chose to fit data points closer to the CO_2 feature. For the sources where the $^{13}CO_2$ feature was detected, separate continuum determinations were made for this feature in a way analogous to that for the main isotopic form.

Since there is wider spectral coverage for RAFGL 989, we made a global continuum fit between 2.4 and 6 μm for this source. The spectrum contains a very broad (~ 700 cm^{-1}) absorption feature peaking at 4.5 μm, attributed to the H_2O-ice combination mode ($3\nu_L$ and/or $\nu_2 + \nu_L$, where L indicates libration), superposed on the 4.27 μm feature. We removed the contribution arising from this feature by making a least-χ^2 fit of a laboratory spectrum of water to the 3 μm feature. The $\tau \sim 0.035$ combination mode was then subtracted from the optical depth plot.

In Elias 16 and possibly also Elias 13, both of which are K-type giants, the interstellar spectrum is superposed on absorption in the $v = 3 \rightarrow 2$, $2 \rightarrow 1$, and $1 \rightarrow 0$ bandheads of CO, at 4.41, 4.35, and 4.295 μm, respectively (Goorvitch 1994; Whittet et al. 1998; Boogert et al. 2000a) that originate in the stellar photospheres. The optical depths of these features are ~ 0.15. To correct for this, an *ISO* spectrum covering the relevant wavelength band of Arcturus (α Bootis), a K1.5 III giant, was subtracted from the Elias 16 spectrum (Fig. 2). The Arcturus spectrum was subtracted "as is"; no attempt to scale the spectrum to fit the absorptions in Elias 16 was made. The 4.34 μm absorption feature is thus canceled out completely, whereas most of the 4.295 μm feature remains after subtraction, indicating the presence of yet another, unidentified feature with peak optical depth ~ 0.2 at 4.295–4.300 μm, or simply a deeper CO absorption in Elias 16 than in Arcturus. The 4.41 μm feature partly overlaps the $^{13}CO_2$ stretch feature (see § 3.3). Because

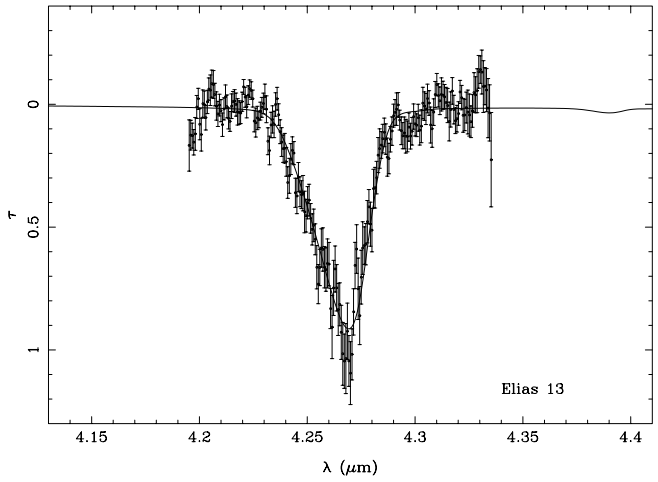

Fig. 1*a*

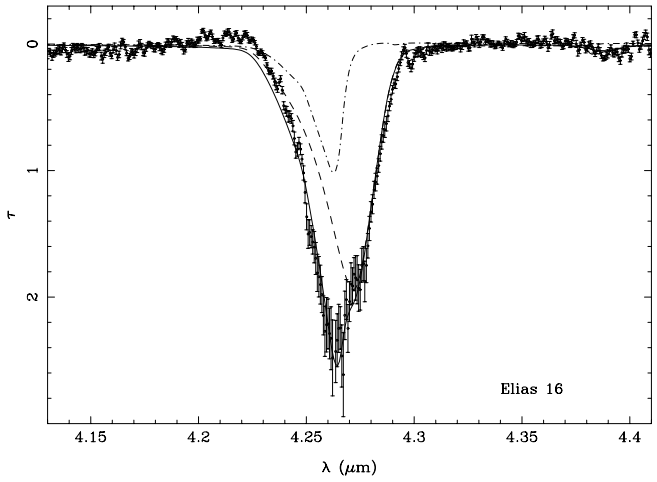

Fig. 1*b*

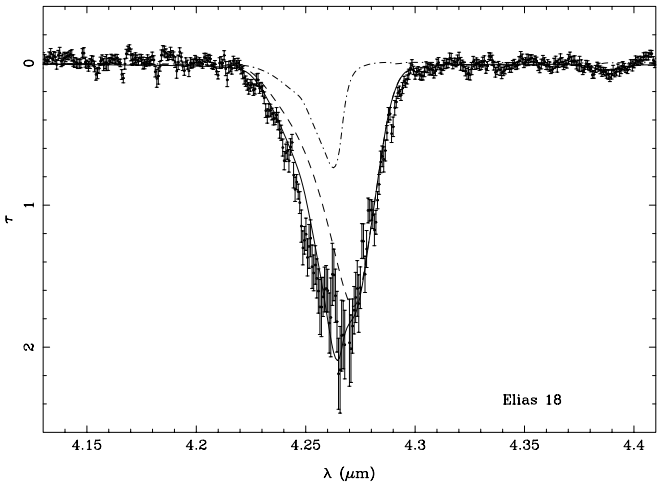

Fig. 1*c*

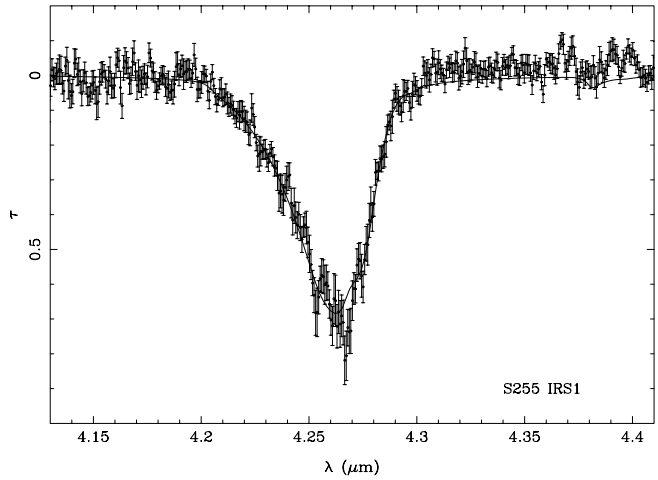

Fig. 1*d*

FIG. 1.—Observed SWS spectra: τ is optical depth and λ wavelength in micrometers. All error bars are 1 σ. Solid lines are the laboratory profiles found to give the best numerical fits to the data in the least-squares norm (see Table 3). For spectra with two-component fits, dashed lines correspond to polar (H_2O-rich) ice, and the dash-dotted-dashed lines correspond to apolar (H_2O-poor) ice.

of the limited wavelength coverage in Elias 13, we did not attempt any correction for photospheric CO in this source.

3. ANALYSIS AND RESULTS

3.1. *Abundance of* CO_2

Column densities of CO_2 ice were determined using

$$N(\mathrm{CO_2}) = \frac{\int \tau_\nu \, d\nu}{A_{4.27}}, \tag{6}$$

where ν is the wavenumber in cm^{-1}, τ_ν is the (unitless) optical depth spectrum, and $A_{4.27}$ is the band strength of the CO_2 ν_3 feature in centimeters per molecule. The band strength depends on the ice mixture in which the CO_2 exists. Gerakines et al. (1995) investigated this dependence for six different mixtures in addition to pure CO_2 ice and found less than 10% variation in $A_{4.27}$ for these ices, with no clear trend in increasing or decreasing band strength between apolar ices versus polar ices. We adopted the band strength to be 7.6×10^{-17} cm molecule^{-1}, corresponding to the value for pure CO_2 ice. In all of the sources the integration was done over the entire absorption profile including wings, where present, which in most cases corresponded to a wavelength range of 4.22–4.33 μm. The resulting column densities are listed in Table 2. Error limits are 1 σ, referring to the flux uncertainty owing to noise only. Additional errors owing to the uncertainty in the estimated continuum levels are also present, in particular, for the sources with very limited spectral coverage such as Elias 13 and HH 57 IRS. These errors should be relatively small, although they are difficult to estimate quantitatively.

For consistency, the H_2O column densities given in Table 2, which were used to calculate the relative CO_2 abundances, all refer to the 3.05 μm O-H stretching mode.

3.2. *Analysis of the* CO_2 *Feature Profiles*

Comparison of the 4.27 μm line profiles (Figs. 1 and 3) separates the objects into two groups. In S255 IRS1 the feature is more sharply peaked than in the other sources, and its short-wavelength wing is more flared. This spectrum is similar to that of other high-mass YSOs observed by Gerakines et al. (1999), e.g., RAFGL 2136. The line profile toward RAFGL 989 shares some characteristics with S255 IRS1, such as the flared short-wavelength wing, but the lack of data points with adequate S/N near the peak of the absorption precludes more detailed comparison. All other

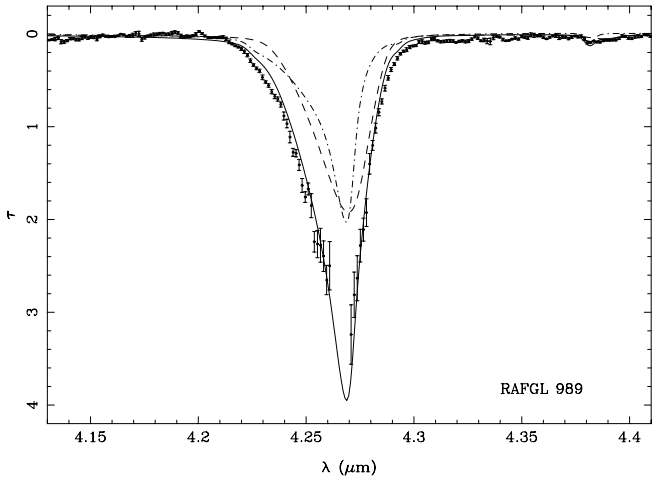

Fig. 1*e*

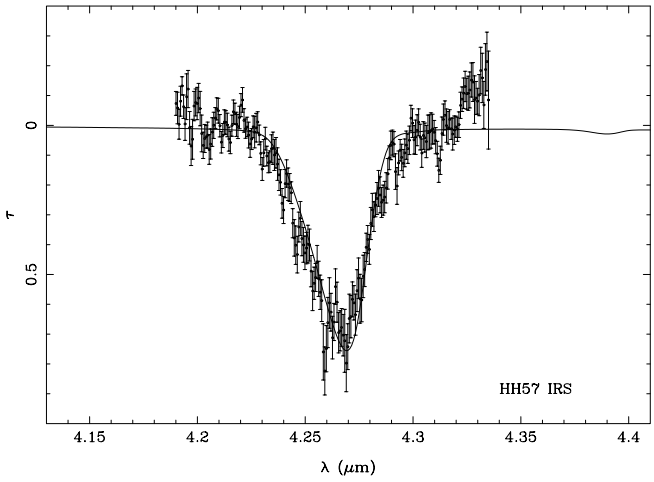

Fig. 1*f*

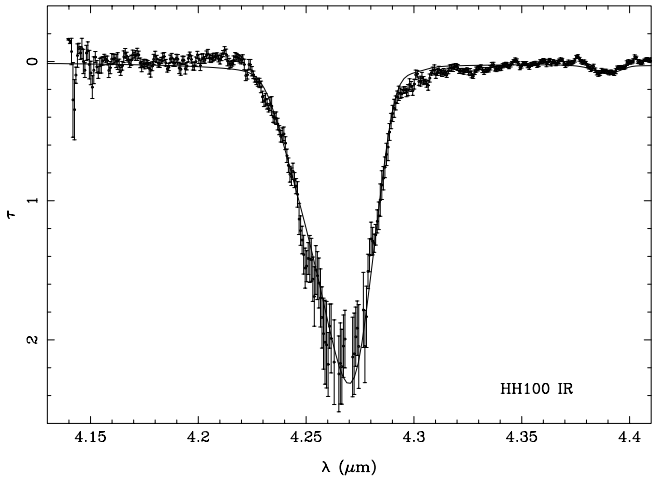

Fig. 1*g*

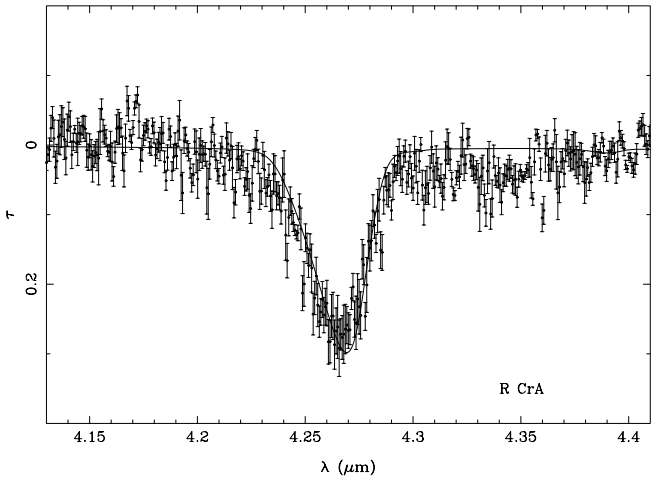

Fig. 1*h*

sources—low-to-intermediate mass YSOs and field stars—have CO_2 line profiles that are remarkably similar to each other. Only subtle differences are present within this group of objects; HH 100 IR and Elias 16, for example, both have

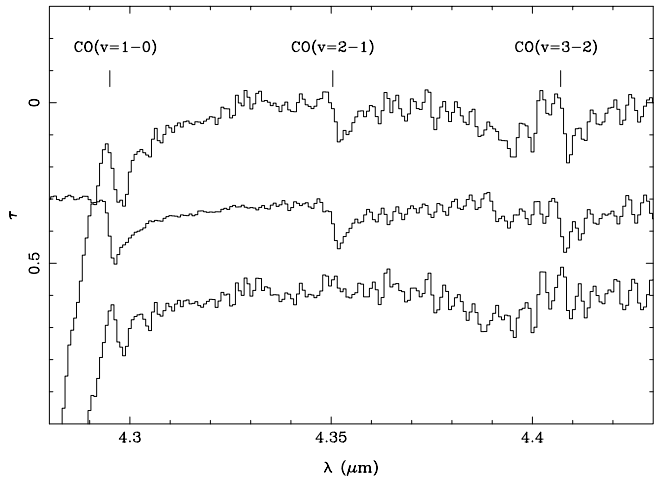

FIG. 2.—*ISO* spectra of the K stars Elias 16 (*upper*) and Arcturus (*middle*), with the CO bandheads indicated. Line positions were taken from Goorvitch (1994). The lower curve is the spectrum of Elias 16 with the Arcturus spectrum subtracted. There are no visible photospheric lines overlapping the solid CO_2 feature itself.

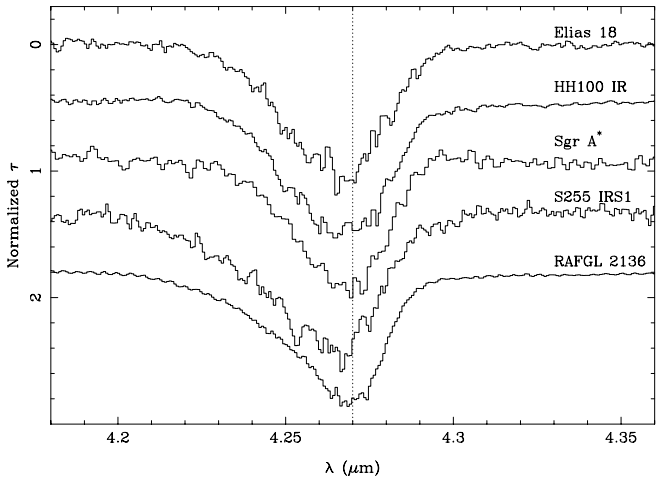

FIG. 3.—Comparison of the 4.27 μm CO_2 line profiles toward two low-mass YSOs, Elias 18 and HH 100 IR, and two high-mass YSOs, S255 IRS1 and RAFGL 2136; also included for comparison is the Galactic Center source Sgr A* (Gerakines et al. 1999; Chiar et al. 2000). Low-mass YSOs, of which Elias 18 and HH 100 IR are good examples, have 4.27 μm profiles very similar to those toward pure background sources (Elias 13, Elias 16, and also Sgr A*). S255 IRS1 (and also RAFGL 989) are more similar to RAFGL 2136 (see Gerakines et al. 1999).

TABLE 2

LINE-OF-SIGHT AVERAGED ICE COLUMN DENSITIES

Line of Sight	$N(CO_2)^a$ (10^{17} cm^{-2})	$N(^{13}CO_2)^a$ (10^{15} cm^{-2})	$N(H_2O)$ (10^{18} cm^{-2})	$N(CO)$ (10^{17} cm^{-2})	$N(CH_3OH)$ (10^{17} cm^{-2})	$\frac{N(CO_2)}{N(H_2O)}$ (%)	References
Elias 13	2.1 ± 0.4	...	1.1	0.9	<0.2	19	1, 2, 3
Elias 16	5.8 ± 0.5	9.2 ± 3.6	2.5	6.5	<0.8	23	1, 2, 3
Elias 18	5.2 ± 0.4	6.3 ± 3.9	1.4	2.3	<0.8	37	1, 2, 3
S255 IRS1	2.2 ± 0.2	...	2.5	...	...	9	4
RAFGL 989.....	8.1 ± 0.1	10.3 ± 26.3	2.4	4.3	<1.7	34	5, 6
HH 57 IRS	1.9 ± 0.4	...	0.9	...	<1.0	21	7
HH 100 IR	6.2 ± 0.6	8.6 ± 2.4	2.4	6.2	2.4	26	8, 9
R CrA	0.9 ± 0.1	...	0.3	<0.4	<1.6	30	10

[a] Adopting $A = 7.6 \times 10^{-17}$ cm molecule^{-1} and $A = 7.8 \times 10^{-17}$ cm molecule^{-1} for the $^{12}CO_2$ and $^{13}CO_2$ ν_3 bands, respectively (Gerakines et al. 1995).

REFERENCES.—(1) Whittet et al. 1998; (2) Chiar et al. 1995; (3) Chiar, Adamson, & Whittet 1996; (4) estimated from Smith, Sellgren, & Tokunaga 1989; (5) this paper: $N(H_2O)$ estimated by fitting a 30 K pure H_2O lab profile to the 3 μm OH-stretch feature, using $A = 2 \times 10^{-16}$ cm molecule^{-1}; (6) this paper: $N(CO)$ inferred from 4.67 μm *ISO* spectrum using $A = 1.1 \times 10^{-17}$ cm molecule^{-1}; (7) estimated from Graham 1998; (8) Whittet et al. 1996; (9) chiar et al. 1998; (10) estimated from Tanaka et al. 1994.

very shallow ($\tau < 0.1$) wings extending to 4.32–4.33 μm, not seen in, e.g., Elias 18, despite comparable S/N. Similar superposed, broad spectral features have previously been seen in other lines of sight, e.g., by Gerakines et al. (1999). Other than this, no significant difference could be detected between the spectra of low-mass YSOs and those of pure background objects such as Elias 13 and Elias 16. This correspondence extends also to the Galactic Center object Sgr A* (Fig. 3), likewise a background source seen through foreground molecular cloud material.[3]

It has been established observationally that both CO and CO_2 can exist in ices of chemically diverse compositions (e.g., Tielens et al. 1991; Whittet et al. 1998; Gerakines et al. 1999). To investigate what physical and chemical constraints can be placed by our 4.27 μm spectra on the environment of the CO_2 molecules, laboratory spectra of interstellar ice analogs containing CO_2 were matched to the *ISO* data. The peak position, width, and shape of the CO_2 stretching mode depend on the chemical composition and temperature of the ice matrix containing the CO_2 (although to a lesser degree than the 15 μm bending mode; see § 1). We used the laboratory spectra from the Leiden Observatory Laboratory (Ehrenfreund et al. 1996, 1999).[4] This database contains spectra from basically three different types of ices: polar, apolar, and annealed. In the polar ices, molecules with high dipole moments such as H_2O and CH_3OH are the main constituents, whereas apolar ices consist of mainly CO, O_2, N_2, or CO_2 itself. The annealed ices have been slowly warmed up to allow recrystallization.

Laboratory profiles were compared to the observed 4.27 μm features using a least-squares method, in which the peak optical depth of the laboratory spectrum was used as a free parameter. An unweighted fitting procedure was found to produce fits that were more acceptable to the eye than procedures where each data point was weighted with its sigma, and was therefore preferred. Both single ice components (polar, apolar, or annealed) and binary combinations (polar/apolar or polar/annealed) were tried for all the available ice temperatures. In addition to the results from the formal least-squares fitting procedure, we also took into account observed abundances and upper limits of ice species other than CO_2 (e.g., CO, CH_3OH) when selecting the most suitable ice mixture.

Results from the least-squares fitting suggest that the 4.27 μm CO_2 feature is not by itself sufficient to identify a *unique* ice mixture to represent the data along any given line of sight, as several different laboratory spectra can produce almost the same formal goodness of fit. However, qualitative conclusions may still be drawn on the types of ice mixtures present. Of course, better fits were achieved using polar/apolar or polar/annealed ice combinations on account of having two free parameters. However, in several of the sources the improvement in the quality of the fit was regarded as insufficient[5] to warrant the use of a two-component model, in which case we considered a single ice component to be the most appropriate representation of the data. The laboratory ices thus chosen are given in Table 3 and displayed in the optical depth spectra in Figure 1.

An important point to consider is that the laboratory spectra used here were obtained by transmission spectroscopy of thin ice films. As is well known, the size, shape, and composition of interstellar grains, as well as the optical properties of the ice, affect ice absorption profiles through Mie scattering (e.g., Bohren & Huffman 1983; Tielens et al. 1991; Ehrenfreund et al. 1997) so that comparison between interstellar and laboratory spectra is not straightforward (e.g., Baratta, Palumbo, & Strazzulla 2000). This effect is particularly pronounced for bands with high intrinsic strengths, such as the CO_2 stretch. To estimate the impact of scattering on the 4.27 μm profile, we used the spectra calculated and tabulated for four different grain models for the polar and apolar ices in the Leiden database to fit the *ISO* data (only single ice components were attempted). The four cases were (1) spherical grains, (2) a distribution of ellipsoidal grains with each particle shape equally probable (continuous distribution of ellipsoids [CDE]), (3) spherical grains coated with H_2O/CO_2 mantles, where the grains and mantles are of equal volume, and (4) a distribution of spherical silicate grains with an ice mantle of constant thickness (denoted "MRN" in the Leiden database). We refer to

[3] We note, however, that the *ISO*-SWS aperture centered on Sgr A* also contains M giants, supergiants, and H II regions (Chiar et al. 2000).

[4] See the Leiden Observatory Laboratory Web site at http://www.strw.leidenuniv.nl/~lab.

[5] A deviation of ~20% or less from the best goodness-of-fit value was used as a rule of thumb.

TABLE 3

FITTING RESULTS

Object	Mixture(s)	T (K)	τ
Elias 13	$H_2O:CO_2 = 100:10$	10	0.91
Elias 16	$H_2O:CO_2:CO = 100:20:3/CO:N_2:CO_2 = 100:50:20$	20/30	1.94/1.02/2.54[a]
Elias 18	$H_2O:CO_2:CO = 100:20:3/CO:N_2:CO_2 = 100:50:20$	20/30	1.71/0.74/2.09[a]
S255 IRS1	$H_2O:CH_3OH:CO_2 = 20:6:10$	112	0.68
RAFGL 989.....	$H_2O:CO_2 = 100:14/H_2O:CO:CO_2 = 1:50:56$	10/45	1.92/2.03/3.95[a]
HH 57 IRS.....	$H_2O:CO_2 = 100:10$	10	0.76
HH 100 IR	$H_2O:CH_3OH:CO_2 = 9:1:2$	10	2.31
R CrA	$H_2O:CO_2 = 100:10$	10	0.30

NOTE.—τ is the optical depth found by fitting laboratory profiles to the *ISO* data. All optical depths tabulated are peak values.

[a] Polar/apolar/total optical depth.

Ehrenfreund et al. (1997) and references therein for details of these different models.

For ices where CO_2 itself is present at low concentration ($\sim$25% or less), we find the discrepancy between the CO_2 stretch feature for the four different grain models to be relatively small (see also the results for CO by Tielens et al. 1991). An example is shown in Figure 4, in which corrected and uncorrected spectra are plotted for an $H_2O:CO_2 = 100:14$ mixture at 10 K. Similarly small differences between the grain models were observed for, e.g., $H_2O:CO_2:CO = 100:20:3$. Hence, given the spectral resolution and S/Ns in the present *ISO* data and the uncertainty of the ice optical constants, we believe that particle shape corrections will not significantly change the results for these ices. However, for ices consisting purely or mainly of CO_2 we find that the four grain models in the Leiden database diverge, in many cases dramatically. Whether this is strictly because of real physical effects, or perhaps owing to physical effects in combination with a lower numerical accuracy for these ices, e.g., because of the sharper CO_2 features, is unknown to us. However, spikes that appear to be numerical artifacts are present in some of these calculated spectra. Furthermore,

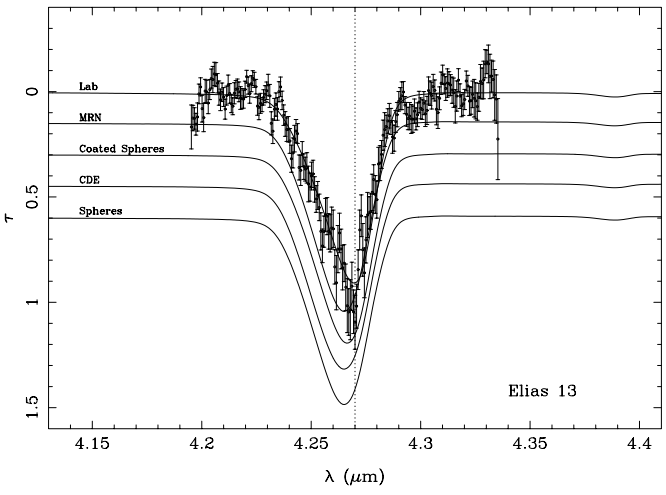

FIG. 4.—Comparison of the 4.27 μm CO_2 line profile for a thin film spectrum obtained in the laboratory ("Lab") and four spectra from the Leiden database that have been corrected for Mie scattering using four different grain models ("MRN," "Coated Spheres," "CDE," and "Spheres," respectively, displaced vertically for display). The spectra are all for an $H_2O:CO_2 = 100:14$ ice mixture at 10 K. Also shown for comparison is the observed profile in Elias 13. The vertical dotted line at 4.27 μm is for easier comparison.

none of the scattering-corrected spectra produces a fit to the *ISO* data that is any better than the uncorrected, thin film laboratory data for the ices studied. One of the ices affected by this is the $H_2O:O_2:CO_2 = 1:50:56$ mixture, which is the apolar component of the combination found to give a good fit to the data for RAFGL 989 (Table 3). Hence, this particular mixture should be regarded with scepticism. The methanol-rich, annealed laboratory ices are segregated, and as a result they are not well represented by thin films (Ehrenfreund et al. 1999); because of this, no particle-shape corrections are appropriate for these data (Gerakines et al. 1999).

The spectra of Elias 13, HH 57 IRS, and R CrA can be well represented by a single, polar ice component. The Elias 13 spectrum is best represented by an ice with $H_2O:CO_2$ in a 100:10 or 100:14 mixture at 10–40 K, with the best fit obtained at 10 K. No mixtures containing CH_3OH, or ices at temperatures higher than $\sim$40 K, fit this spectrum well. HH 57 IRS can be fitted by low-temperature ices: $H_2O:CO_2 = 10:1$ (10–30 K), or $H_2O:CH_3OH:CO_2 = 9:1:2$ (10–45 K). It is also well fitted by $CO_2:CH_3OH = 1:2$ and 1:3 at 125 K and $H_2O:CH_3OH:CO_2 = 11:12:10$ at 10 K, but these mixtures disagree with the observed upper limit on the methanol abundance. R CrA can be equally well fitted by a whole suite of $H_2O:CH_3OH:CO_2$ ice mixtures in various proportions and at a wide range of temperatures up to about 120 K, including the 10 K $H_2O:CO = 10:1$ ice found to give good results for several of the other stars. This line of sight is probably the most poorly constrained.

Elias 16, Elias 18, and RAFGL 989 are all best fitted by combinations of polar and apolar ices, as listed in Table 3. The binary mixture in Elias 16 also gives a CO column density that is consistent with observations. The Elias 18 spectrum can be equally well fitted by the 10 K methanol-containing ice mixture used for HH 100 IR, but this ice would imply a methanol abundance that is inconsistent with the observed upper limit (from 3.5 μm data; see Table 2).

Finally, HH 100 IR and S255 IRS1 are both best fitted by methanol-containing ices. Toward HH 100 IR either a combination of a $H_2O:CO_2 = 10:1$ and an $H_2O:CH_3OH:CO_2 = 12:7:10$ mixture, both at 10 K, or a single 10 K $H_2O:CH_3OH:CO_2 = 9:1:2$ mixture works well. The latter also agrees well with the observed abundance of methanol in this line of sight. S255 IRS1 can be well represented by a suite of higher temperature CO_2 and

CH_3OH–bearing ice mixtures with or without H_2O: good fits are obtained with CO_2 :CH_3OH ice in proportions 1:1 at 120 K, 2:1 at 125–145 K, and 3:1 at 112 K; also H_2O:CH_3OH:CO_2 ice in mixtures 4:6:10 at 125 K, 2:6:10 at 112 K (best numerical fit), and 7:7:10 at 120 K gave good fits. This star cannot be adequately fitted by either the H_2O:CO_2 = 10:1 mixture that fits well in most of the lower mass sources or by low-temperature ices because of the extended blue wing of the absorption line. Again, we emphasize that these results are only qualitative and should in no way be considered unique solutions.

Further constraints on the ice composition could be provided by the $^{13}CO_2$ stretch band detected in Elias 16, Elias 18, HH 100 IR, and RAFGL 989 (see Boogert et al. 2000a). However, the weakness of this band in our source sample prevents confident identification of features characteristic of different ice mixtures and, thus, does not narrow down the possible ice mixtures significantly.

At the resolution of the SWS06 spectra any rotational structure of gas-phase CO_2 would, if present, be barely resolved. The position of the gas-phase ν_3 stretch essentially coincides with the solid state equivalent so that the *P*- and *R*-branch rovibrational structure would be superposed on the solid feature (van Dishoeck et al. 1996; Helmich 1996). No such structure was recognized in any of the observed sources, and the fraction of the absorption at 4.27 μm coming from CO_2 gas along the line of sight must therefore be small in all sources, similar to what was found by van Dishoeck et al. (1996).

3.3. *Abundance of* $^{13}CO_2$

The 4.39 μm ν_3 band of solid $^{13}CO_2$ was detected in Elias 16, Elias 18, HH 100 IR, and RAFGL 989. The 4.39 μm feature in Elias 16 overlaps the photospheric CO line at 4.407 μm, but the latter is effectively removed by subtraction of the Arcturus spectrum (see § 2). Column densities of $^{13}CO_2$ ice were calculated using equation (6), with the band strength set to 7.8×10^{-17} cm molecule^{-1} (Gerakines et al. 1995). Integration was done over the entire line profile, i.e., approximately 4.37–4.41 μm. Results are given in Table 2. The uncertainties of these estimates are quite large because of the intrinsic weakness of the feature and the limited S/Ns, and this also precludes detailed analysis of the line profiles.

Our data infer $^{12}CO_2/^{13}CO_2$ ratios of 57^{+54}_{-16}, 83^{+150}_{-36}, $79^{+\infty}_{-57}$, and 72^{+38}_{-21} for Elias 16, Elias 18, RAFGL 989, and HH 100 IR, respectively. Although these results have large uncertainties for reasons already noted, the nominal values are in agreement with $^{12}C/^{13}C$-values measured for local interstellar gas (e.g., Wilson & Rood 1994) and with the results found by Boogert et al. (2000a) in their extensive study of $^{13}CO_2$.

4. DISCUSSION AND CONCLUSIONS

The data presented here suggest that most of the CO_2 is located in cold, predominantly polar ice mantles with $CO_2/H_2O \sim 0.1$–0.2. These mantles are present in both the quiescent intracloud medium and in the environs of the low-to-intermediate mass YSOs in our sample. The presence of an embedded source of moderate mass, such as Elias 18 or HH 100 IR, has no strong impact on the profile of the ν_3 stretch band as compared to pure background objects such as Elias 13, Elias 16, and Sgr A*, where there is no significant interaction with the absorbing dust, and the corresponding ice mantles therefore seem to represent a very similar state of processing. Considering the large dust columns toward these objects, a significant fraction of the CO_2 absorption could arise in cloud material unrelated to the YSOs themselves.

In the line of sight toward what is probably the most massive object in our study, S255 IRS1, the CO_2 seems to be located in a warmer, thermally processed ice mixture that is rich in CO_2 and contains trace amounts of methanol (Table 3). The relatively high CO_2/H_2O concentration (50%) in the selected mixture, compared with the line-of-sight average (9%), is readily explicable in terms of either segregation within the ice mantles or the existence of substantial chemical gradients along the line of sight (perhaps both). Formal fitting of laboratory data to the line profile of RAFGL 989 selects a polar/apolar combination rather than an annealed methanol-containing ice but with lower confidence for reasons already noted. Both S255 IRS1 and RAFGL 989 have line profiles that resemble that of, e.g., RAFGL 2136 (Gerakines et al. 1999) much more closely than those of objects of lower mass.

The relatively high concentrations of CO_2 relative to H_2O (19%–26%) observed toward field stars Elias 13 and Elias 16 and low-mass YSOs such as HH 100 IR, HH 57 IRS (this paper), and Elias 29 (Boogert et al. 2000b) confirms the earlier result of Whittet et al. (1998) that CO_2 can be efficiently formed without processing by an embedded luminous source. If UV processing is the driving mechanism in the production of CO_2 in interstellar ices, as suggested by laboratory studies, then an appreciable UV field must exist inside the clouds. This might be produced through cosmic-ray–induced fluorescence of molecular hydrogen or by penetration of the interstellar UV field at a level strong enough to maintain photochemistry (see discussion by Whittet et al. 1998). Most of the CO_2 absorption could, for example, occur near cloud edges so that there are strong abundance gradients along the line of sight. Alternatively, bombardment of cosmic-ray ions could perhaps drive the CO_2 chemistry directly. Recent laboratory experiments indicate that UV photons and high-energy protons can contribute equally to the production of certain molecules under simulated interstellar conditions (Moore, Hudson, & Gerakines 2001), although CO_2 was not specifically studied. Alternatively, diffusive grain surface reactions could play an important role for CO_2 production, but in the absence of reliable diffusion rates and activation barriers, their importance is hard to estimate quantitatively (see § 1.2).

The correlation between CO_2 and H_2O column densities (Fig. 5) shows source-to-source variation greater than seen in previous studies. For the embedded B-type stars Elias 18 and RAFGL 989, we find very high (34%–37%) CO_2 concentrations; they both deviate by a factor of $\sim$2 from the correlation line of Gerakines et al. (1999). For comparison, the solid CO abundances relative to H_2O toward Elias 18 (Chiar et al. 1995, 1998) and RAFGL 989 (Tielens et al. 1991) are 16%–18%, intermediate between those typically observed in high-mass objects (<10%) and intracloud regions (Elias 16: 23%). The lines of sight toward Elias 18 and RAFGL 989 could therefore sample material cold enough to retain some solid CO, in which UV irradiation may drive photochemical oxidation of CO to CO_2. Indeed, the presence of a very weak 4.62 μm "XCN" feature toward Elias 18 (Tegler et al. 1995) does indicate some energetic processing in this source. In contrast to Elias 18 and RAFGL 989, the massive YSO S255 IRS1 is deficient in

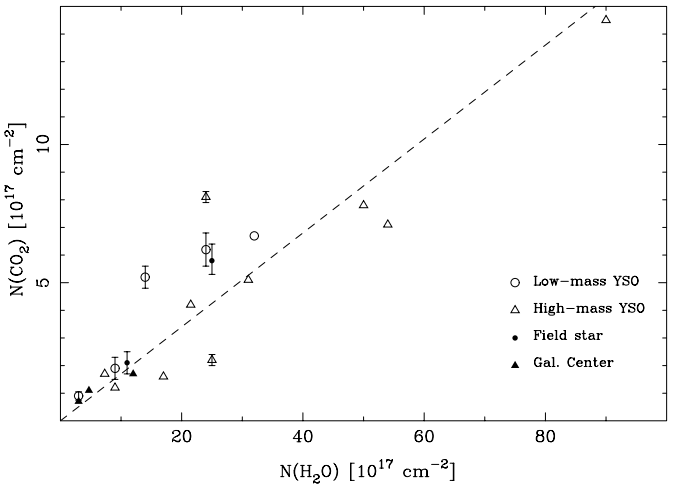

FIG. 5.—Column density plot of solid CO_2 vs. solid H_2O for 20 sources. Symbols with error bars (indicating 1 σ) represent objects studied in this paper. All other objects were taken from the study of Gerakines et al. (1999; RAFGL 7009S is off scale in this plot). *Open circles*: low-mass YSOs; *filled circles*: background stars; *open triangles*: intermediate- and high-mass YSOs; *filled triangles*: Galactic Center sources. The dashed line indicates the correlation $N(CO_2) = 0.17N(H_2O)$ found by Gerakines et al. (1999) for their sample.

CO_2 (9%) compared to the objects of lower mass. It is thus interesting to note that S255 IRS1 and RAFGL 989 represent the lowest and highest CO_2 concentrations, respectively, despite having very similar line profiles. A possible explanation of the CO_2 deficiency toward S255 IRS1 could of course be a higher rate of photodissociation of CO_2 because of the higher luminosity of this YSO, or perhaps a later evolutionary state, but this does not explain why it is different from similarly massive objects such as RAFGL 2136.

The results presented in this paper provide motivation for further development of gas-grain chemistry models of dark quiescent clouds, and laboratory studies of diffusion rates and activation barriers of key grain surface reactions, in order to assess the importance of such reactions for the chemistry of interstellar ice mantles. We also note that 15 μm spectra of the CO_2 bending mode toward objects reported in this paper may ultimately be obtained with the infrared spectrometer of the *Space Infrared Telescope Facility*, albeit at lower resolution than that attainable with the *ISO*-SWS.

We would like to thank Eric Herbst and Deborah Ruffle for providing papers prior to publication, and Ewine van Dishoeck, Willem Schutte, and Pascale Ehrenfreund for helpful comments on various versions of the manuscript. Financial support from the New York Center for Studies on the Origins of Life via NASA grant NAG 5-7598 is gratefully acknowledged. J. E. C. is supported by NASA's Long-Term Space Astrophysics program under grant 399-20-61-02. *ISO* data reductions were supported by NASA through JPL contract 961624. The data presented were analyzed with the support of the Dutch *ISO* Data Analysis Centre (DIDAC) at the Space Research Organization of the Netherlands (SRON) in Groningen, the Netherlands.

REFERENCES

Allen, D. A. 1972, ApJ, 172, L55
Axon, D. J., et al. 1982, MNRAS, 200, 239
Baratta, G. A., Palumbo, M. E., & Strazzulla, G. 2000, A&A, 357, 1045
Bastien, P., & Ménard, F. 1990, ApJ, 364, 232
Bohren, C. F., & Huffman, D. R. 1983, Absorption and Scattering of Light by Small Particles (New York: John Wiley & Sons)
Boogert, A. C. A., et al. 2000a, A&A, 353, 349
———. 2000b, A&A, 360, 683
Boonman, A. M. S., van Dishoeck, E. F., Lahuis, F., Wright, C. M., & Doty, S. D. 2000, in *ISO* Beyond the Peaks: The Second *ISO* workshop on Analytical Spectroscopy, ed. A. Salama, M. F. Kessler, K. Leech, & B. Schulz (ESA-SP 456; Noordwijk: ESA), 67
Charnley, S. B., & Kaufman, M. J. 2000, ApJ, 529, L111
Chiar, J. E., Adamson, A. J., Kerr, T. H., & Whittet, D. C. B. 1995, ApJ, 455, 234
Chiar, J. E., Adamson, A. J., & Whittet, D. C. B. 1996, ApJ, 472, 665
Chiar, J. E., Gerakines, P. A., Whittet, D. C. B., Pendleton, Y. J., Tielens, A. G. G. M., & Adamson, A. J. 1998, ApJ, 498, 716
Chiar, J. E., et al. 2000, ApJ, 537, 749
de Graauw, Th., et al. 1996a, A&A, 315, L345
———. 1996b, A&A, 315, L49
d'Hendecourt, L. B., Allamandola, L. J., Grim, R. J. A., & Greenberg, J. M. 1986, A&A, 158, 119
Ehrenfreund, P., et al. 1996, A&A, 315, L341
———. 1997, A&A, 328, 649
———. 1999, A&A, 350, 240
Elias, J. H. 1978, ApJ, 224, 857
———. 1980, ApJ, 241, 728
Fournier, J., et al. 1979, J. Chem. Phys., 70, 5726
Frost, M. J., Sharkey, P., & Smith I. M. 1991, Faraday Discuss., 91, 305
Gerakines, P. A., et al. 1995, A&A, 296, 810
———. 1999, ApJ, 522, 357
Goorvitch, D. 1994, ApJS, 95, 535
Graham, J. A. 1998, ApJ, 492, 213
Graham, J. A., & Frogel, J. A. 1985, ApJ, 289, 331
Grim, R. J. A., & d'Hendecourt, L. B. 1986, A&A, 167, 161
Gürtler, J., Henning, Th., Pfau, W., Krätschmer, W., & Lemke, D. 1996, A&A, 315, L189
Helmich, F. P. 1996, Ph.D. thesis, Univ. Leiden
Herbst, E., & Leung, C. M. 1986, MNRAS, 222, 689
Hillenbrand, L. A., et al. 1992, ApJ, 397, 613
Howard, E. M., Pipher, J. L., & Forrest, W. J. 1997, ApJ, 481, 327
Moore, M. H., Hudson, R. L., & Gerakines, P. A. 2001, Spectrochim. Acta, 54, 843
Reipurth, B. 1985, A&A, 143, 435
Reipurth, B., & Wamsteker, W. 1983, A&A, 119, 14
Reipurth, B., et al. 1993, A&A, 273, 221
Ruffle, D. P., & Herbst, E. 2001, MNRAS, 322, 770
Sandford, S. A., et al. 1988, ApJ, 329, 498
Schreyer, K., Helmich, F. P., van Dishoeck, E. F., & Henning, Th. 1997, A&A, 326, 347
Shuping, R. Y., Chiar, J. E., Snow, T. P., & Kerr, T. 2001, ApJ, 547, L161
Smith, R. G., Sellgren, K., & Tokunaga, A. T. 1989, ApJ, 344, 413
Tanaka, M., et al. 1994, ApJ, 430, 779
Tegler, S. C., et al. 1995, ApJ, 439, 279
Thompson, R. I., et al. 1998, ApJ, 492, L177
Tielens, A. G. G. M., Tokunaga, A. T., Geballe, T. R., & Baas, F. 1991, ApJ, 381, 181
van den Ancker, M. E., Wesselius, P. R., & Tielens, A. G. G. M. 2000, A&A, 355, 194
van Dishoeck, E. F., et al. 1996, A&A, 315, L349
Weintraub, D. A., Sandell, G., & Duncan, W. D. 1991, ApJ, 382, 270
Whittet, D. C. B., Bode, M. F., Longmore, A. J., Admason, A. J., McFadzean, A. D., Aitken, D. K., & Roche, P. F. 1988, MNRAS, 233, 321
Whittet, D. C. B., et al. 1996, ApJ, 458, 363
———. 1998, ApJ, 498, L159
Wilson, T. L., & Rood, R. T. 1994, ARA&A, 32, 191
Wynn-Williams, C. G. 1982, ARA&A, 20, 587